arXiv:2101.06019v1 [physics.ins-det] 15 Jan 2021

Pixelated 3D sensors for tracking in radiation harsh environments

Jordi Duarte-Campderros[1] on behalf of the RD50 Collaboration

[1]*Instituto de Fisica de Cantabria (IFCA (UC/CSIC)), Av. de los Castros s/n, Santander 39005, Spain*

E-mail: jorge.duarte.campderros@cern.ch

(Received November 26, 2020)

The High Luminosity upgrade of the CERN Large Hadron Collider will be able to reach a peak instantaneous luminosity of $5 \times 10^{34}\,\mathrm{cm}^{-2}\,\mathrm{s}^{-1}$. The innermost detectors of the CMS and ATLAS experiments will have to cope with unprecedented requirements on radiation hardness. At the end of the operation period, radiation levels are expected to reach values above $2.6 \times 10^{16}\,\mathrm{n_{eq}}\,\mathrm{cm}^{-2}$. Sensors based on 3D pixel technology, with intrinsic radiation tolerance, are the baseline option for the innermost layers of the vertex detectors of several HL-LHC experiments. This article gives an overview of the ongoing characterization of the pixelated 3D sensor technology, their performance and their current development status for tracking on radiation harsh environments.

KEYWORDS: particle tracking detectors,HL-LHC upgrade,3D silicon pixel detectors, radiation-hard detector

1. Introduction

The High Luminosity Large Hadron Collider (HL-LHC) project [1] is going to push their experiments to very stringent radiation environments. The innermost detectors of the largest HL-LHC experiments, ATLAS and CMS, will have to cope with unprecedented radiation levels and with extremely high track densities. Their upgraded vertex detectors will have to be able to operate in a hostile radiation environment, reaching hadron fluences up to about $2.6 \times 10^{16}\,\mathrm{n_{eq}}\,\mathrm{cm}^{-2}$ before being replaced [2, 3]. Sensors based on 3D pixel technology are excellent candidates because of their inherent radiation tolerance.

A 3D sensor is built by inserting highly doped columns into the bulk to form the P-N junctions, decoupling in that way the inter-electrode distance from the active sensor thickness (see Fig. 1). The thickness is defining the amount of charge generated but is in the case of 3D sensors independent of the distance between the electrodes, respectively the depletion voltage. The inter-electrode distance can thus be optimized independent of the amount of charge deposited by an ionizing particle, as opposite to a planar sensor. The small inter-electrode distance allows to reduce the charge carrier trapping probability after irradiation, acquire the induced charge faster, and use low voltages to fully deplete the sensor, among other benefits [4]. This low depletion voltage enables to operate the 3D sensors with an extremely low power consumption, especially compared with equivalent planar sensors.

However, the columnar structure also presents some disadvantages. The electric field is not uniform within the depleted region, and therefore the sensor response cannot be uniform either. Indeed, there are charge losses inside the electrodes and ohmic columns, as the columns themselves are not active regions. Null points between same type of electrodes will delay the created charges generated in there, as they have to diffuse first. As the inter-electrode

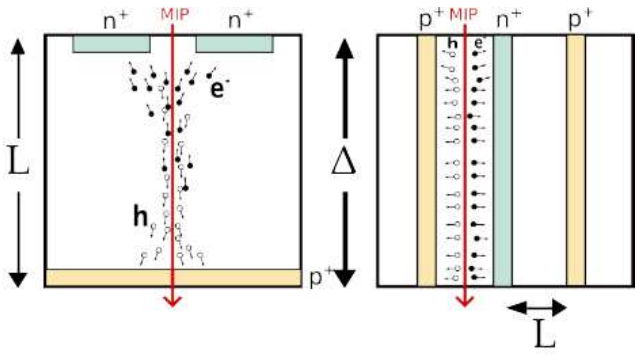


Fig. 1. Schematic simplified layout of a planar (left) and a 3D (right) sensors, assuming a n-in-p layer structure. Read out electrodes are bonded to the highly doped n^+ thin region (colored in green). Electrodes bonded to the ohmic layers p^+ (colored in yellow) are needed to polarize the sensor. The sensor thickness, Δ, determines how many charges are created int the sensor when a particle passes through, while the inter-electrode distance, L, defines the maximum distance a charge carrier should travel before being collected. It can be observed that in a planar sensor $L = \Delta$, but in a 3D sensor $L << \Delta$.

distance is smaller, the capacitance of a 3D sensor is order of 3-5 times higher than an equivalent planar, and consequently a 3D sensor is noisier. The fabrication process is still in the development phase, being an expensive and time consuming process made by just a few R&D institutions or foundries (IMB-CNM in Barcelona, FBK in Trento or SINTEF in Oslo), especially compared to the manufacturing of planar sensors. There are many companies capable to produce planar sensors, and with a well-established production, even for this small-pitch detector.

Several of these drawbacks can be or have been overcome. For instance, the production processes have been simplified and improved over the past few years, in particular by using single-sided processes as opposed to the double-sided initially used for the first 3D batches [5]. The latest productions are mature enough to achieve overall good yields [6]. Another example: the response of the electric field can be *uniformed* by tilting the detector so that the particle passes through different electric field regions.

The 3D pixel technology has already been successfully used in some LHC experiments as position tracking detectors in radiation environments such as in the ATLAS IBL [7], the ATLAS Forward Proton (AFP) detector [8], and the CMS-TOTEM Precision Proton Spectrometer (PPS) detector [9]; proving to be a mature enough yet novel technology. For the HL-LHC, ATLAS already decided to include 3D pixel detectors with $50 \times 50\,\mu m^2$ and $25 \times 100\,\mu m^2$ pixel size in the innermost layer of its new silicon inner tracker [3]. At the time of this report, CMS is in the process of deciding the inclusion of this technology in the two innermost layers of the barrel and in the inner ring of the end-cap of its inner tracking detector.

The RD50 Collaboration has been involved in several activities related with the 3D pixel technology, such as their time performance in order to be used as timing detectors, the radiation hardness at extreme fluences larger than $1 \times 10^{17}\,n_{eq}\,cm^{-2}$, and the qualification and characterization of the small-pitch 3D sensor with the pre-production readout chip RD53A [10], as part of the sensor qualification process for the ATLAS and CMS Phase-2 upgrade programs. The RD50 collaboration has also played an important role to bring 3D sensors to industrial production. In this paper, a summary of the last line of work is being reported. Information and results of the other work packages can be found elsewhere [11–13].

2. Sensor characterization for the HL-LHC experiments upgrade

The inner tracker upgrade projects of ATLAS and CMS require small-pitch, radiation-hard detector candidates, to be assembled with the readout electronics and mechanics projected by the collaborations. The readout chip (ROC) developed for CMS and ATLAS, the RD53A, is a demonstrator ROC for CMS and ATLAS upgrades, based on 65 nm CMOS process [10]. This is a common layout design developed by the RD53 collaboration, which included several Analogs Front-Ends (AFE) to be tested. The CMS and ATLAS ROCs prototypes, the CROC and the ITkPixV1, respectively, have finally chosen to use different AFEs: the linear AFE for CROC and the differential AFE for ITkPixV1. Fig. 2 shows a picture of the RD53A ROC with the linear and differential front-end regions highlighted, and the single chip cards assemblies used for the characterization.

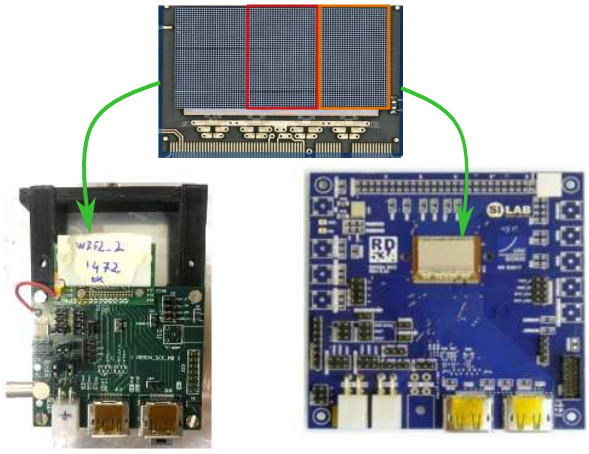


Fig. 2. A RD53A chip picture (top) with the linear and differential regions highlighted in red and orange respectively. The chip bump-bonded to a sensor, is wire-bonded to a single chip card as part of the characterization setup. Two different single chip cards have been used, the RICE card (left, developed by RICE University), and the Bonn card (right, developed by the SiLab group at Bonn University).

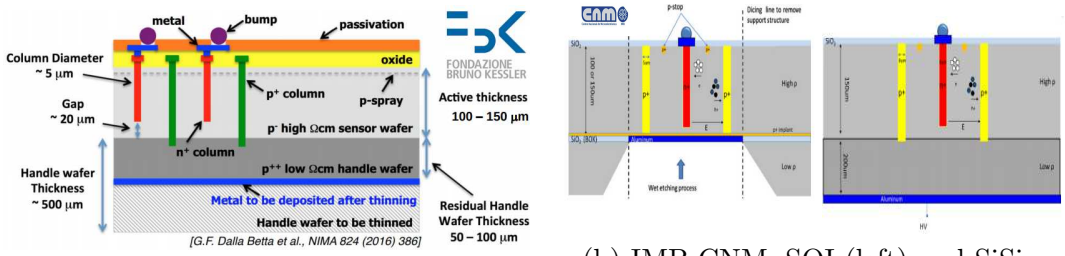
2.1 Module description

The sensors used have been produced either by IMB-CNM in Barcelona (Spain) or by the FBK in Trento (Italy). In both cases, the production was made with a single-sided process on p-type substrates Silicon on Silicon (SiSi) or Silicon on Insulator (SOI). The former has finally been chosen over the SOI, as it does not need the removal of the handle-wafer for biasing, which simplifies the production process and improves the yield. FBK used 6 inches Direct Bond Wafers (DBW) with a support wafer made of 500 µm thick Czochralski (CZ) silicon, with less than 1 Ω cm resistivity. The electrodes were implanted by a Deep Reactive Ion Etching (DRIE) process, in a Float Zone (FZ) wafer of high resistivity (higher than 3000 Ω cm) of 130 µm (production with Mask Aligner lithography) and 150 µm (production with Stepper lithography) thickness. The columns have about 5 µm of diameter.

For the case of the IMB-CNM, the p-type substrates were produced on 4 inches SOI wafers or 4 inches SiSi wafers with a handle wafer of 300 µm thick CZ silicon of low resistivity. The electrodes are implanted on an active region with a nominal resistivity between 1000-5000 Ω cm and 150 µm thick. On the SiSi wafers, there is no need to remove the handle wafer

for bias, as the low-resistivity wafer is conductive. The columns have a diameter of about 8 µm.

Fig. 3 summarizes schematically the described sensors.



(a) FBK

(b) IMB-CNM, SOI (left) and SiSi (right)

Fig. 3. Sensor cross-section layout. The main components are schematized, showing the active region (light gray, high-resistive layer), the support CZ layer (dark gray), the highly-doped column implant (red) and the ohmic columns (green, yellow).

The sensors were manufactured with rectangular and square geometries, matching the layouts CMS and ATLAS are considering to use. The square $50 \times 50\,\mu m^2$ has an inter-electrode distance of about 35 µm, and is the easiest to produce. Furthermore, they do not suffer from the cross-talk originated in the metallic routes [14], needed to match the RD53A $50 \times 50\,\mu m^2$ bond matrix pattern. However, a rectangular geometry allows to increase the resolution in the short pitch side, and therefore were considered as well. Two rectangular geometries $25 \times 100\,\mu m^2$ have been tested: with 2 electrodes (2E) per pixel cell with a very small inter-electrode distance of 28 µm but difficult to produce, and 1 electrode (1E), less problematic to produce but with larger inter-electrode distance. The later has been proven to be enough radiation hard, even with its 52 µm of inter-electrode distance, and therefore the 2E flavour has already been discarded. Fig. 4 summarizes all the pixel geometries used in the results presented in this report.

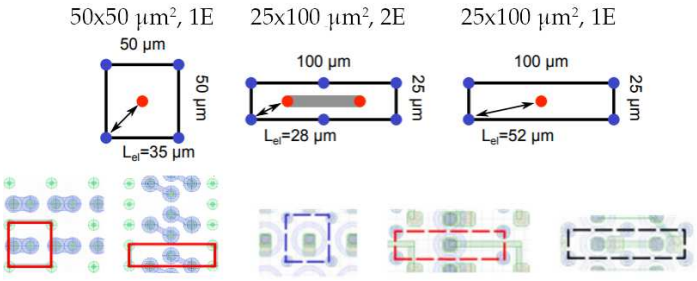


Fig. 4. Pixel geometries considered for CMS and ATLAS. Each pixel cell is defined by the ohmic columns (blue) and the highly doped implant electrode (red). The inter-electrode distance is also specified. The bottom row is showing the different routing pattern used to connect the bond-bumps on the sensor with the RD53A readout electrodes. Solid (for the FBK modules) and dashed (for the IMB-CNM) lines are superimposed to stress a pixel cell.

Some sensors were also irradiated in order to emulate the damage produced by irradiation after years of operation in the experiments. Irradiations have been carried out at several

facilities, with different particles and energies, in several intermediate steps until reaching fluences up to $1 \times 10^{16}\,\mathrm{n_{eq}\,cm^{-2}}$, the expected fluence of the innermost layers of CMS or ATLAS after the two first runs of the HL-LHC in the scenario of $3000\,\mathrm{fb^{-1}}$. Details about the irradiations and methodology can be found in Ref. [15].

2.2 Test beam characterization

Electrical, TCT, TCT-TPA, or other characterizations techniques were used to study the sensors, and results have already been extensively presented elsewhere [13,16,20]. The sensors described in the previous section were bump-bonded to the RD53A demonstrator chip and wire bonded to PCB cards as explained before, and tested under a beam of particles. Two main facilities were used: CERN [17], with hadron beams of $120\,\mathrm{GeV}/c$, and DESY [18], where electrons of $5.6\,\mathrm{GeV}/c$ are delivered to the beam lines. Test beam experiments are useful to study the behaviour and response of a sensor under similar conditions it will face when it is mounted in the real experiment. The sensor response is measured with the help of a telescope [19], where the incident particles are identified and reconstructed. Telescope reconstructed particles are used to identify the position in the sensor under study where a hit should appear, allowing to measure hit-efficiency, charge, resolution, etc.

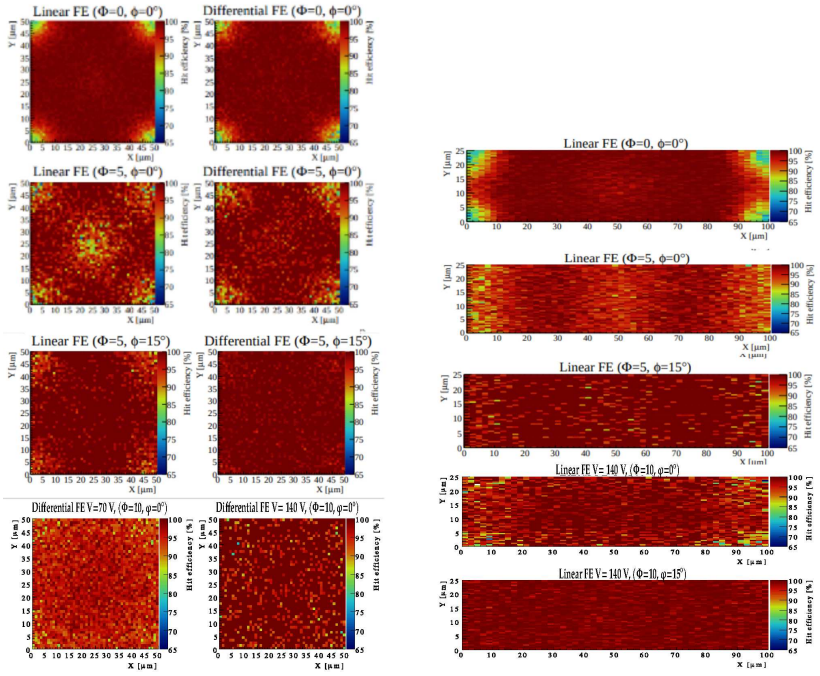
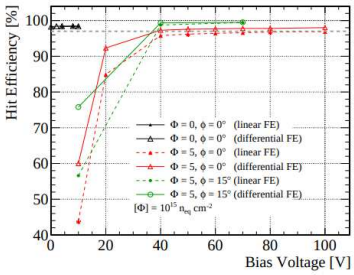


Fig. 5. Hit efficiency per pixel cell in different sensors, shown from left to right; 50x50 Linear and Differential front-end, and 25x100 Linear front-end. From top to bottom are with increasing fluence (Φ) and incident angle of the tracks (ϕ). Details are inserted in the figures, with fluence in units of $1 \times 10^{15}\,\mathrm{n_{eq}\,cm^{-2}}$ (0 for fresh sensors). The operating bias voltaged used is also shown in some plots. Sensors were produced at IBM-CNM with SOI p-type substrates. Figure re-adapted and composed from Ref. [20].

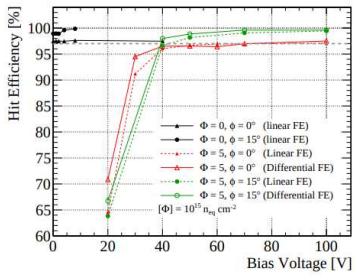
The first important observable reported is the efficiency per pixel cell, measured for $25 \times 100\,\mu\mathrm{m}^2$ and $50 \times 50\,\mu\mathrm{m}^2$ fresh sensors. The two plots in Fig. 5 show the hit efficiency drop in the ohmic columns at the four corners when the incident particles enter perpendicular

to the sensor plane. This drop is the result of the incident particle passing inside the non-active region of the columns. However, there is no significant drop observed in the n-column at center, as the charge generated below the column (see Fig. 3) is enough to create a hit (thresholds are tuned around 1000 electrons).

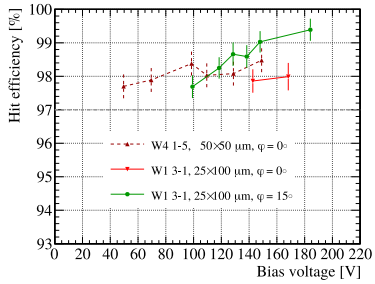
The drop in the n-column appears in the irradiated sensor as consequence of two effects: thresholds are increased to deal with a noisier detector, and trapping, lowering the amount of generated charge below the column. Fresh sensors are exhibiting a 98% overall efficiency, including the ohmic column losses. When tilted, a 99.5% overall efficiency is recovered with very low bias voltages. As it can be observed from Fig. 6, fully depletion is reached with a few volts for fresh sensors, and with a few hundred of volts for sensors irradiated up to $1 \times 10^{16}\,\mathrm{n_{eq}\,cm^{-2}}$.



(a) 50x50, fresh and $5 \times 10^{15}\,\mathrm{n_{eq}\,cm^{-2}}$



(b) 25x100, fresh and $5 \times 10^{15}\,\mathrm{n_{eq}\,cm^{-2}}$



(c) 50x50 and 25x100, $1 \times 10^{16}\,\mathrm{n_{eq}\,cm^{-2}}$

Fig. 6. Measured overall hit efficiency with respect the applied bias voltage, for fresh and irradiated sensors. Figures extracted from [20].

Equivalent results have been obtained for FBK produced sensors [21], showing similar performances (see Fig. 7), as well as similar depletion voltages: sensors irradiated at $1 \times 10^{16}\,\mathrm{n_{eq}\,cm^{-2}}$ fully depletes around 120–150 V.

The resolution of the sensor attached to the RD53A before and after irradiation up to $1 \times 10^{16}\,\mathrm{n_{eq}\,cm^{-2}}$, has been recently measured in the short pixel direction of the $25 \times 100\,\mu\mathrm{m}^2$ geometry [22]. The sensor shows a resolution of 3 µm and there is almost no degradation after irradiation, with a resolution of 5.7 µm evaluated at the optimal angle. These results complement the previously obtained for the $50 \times 50\,\mu\mathrm{m}^2$ geometry, with a resolution of 5 µm, evaluated at the optimal angle and before irradiation.

A parameter of interest, especially important for the commissioning and operation of the modules in the targeted experiment, is the power consumption. The ATLAS specifications are requiring to be below $10\,\mathrm{mW/cm^2}$, while CMS requires less than $1\,\mathrm{W/cm^2}$ (included sensor and chip consumption). The power consumption of the tested sensors after being irradiated up to $1 \times 10^{16}\,\mathrm{n_{eq}\,cm^{-2}}$, has been measured below the ATLAS specifications in the full

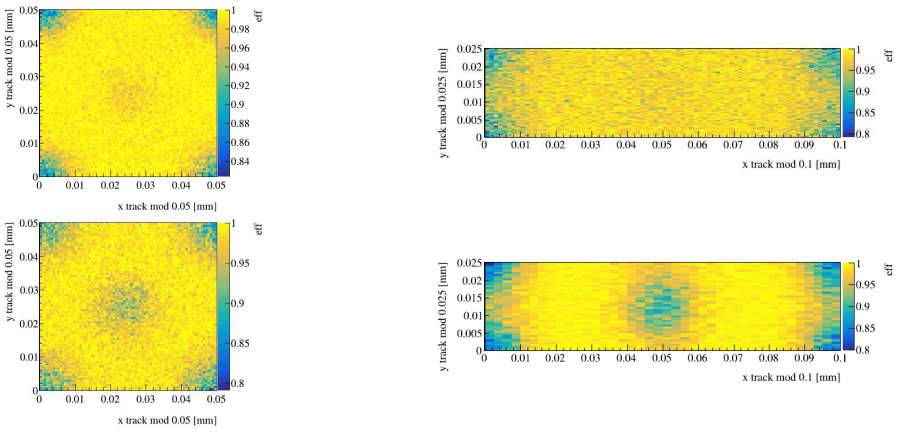


Fig. 7. Hit efficiency in pixel cell for fresh $50 \times 50\,\mu m^2$ (top-left) $25 \times 100\,\mu m^2$ (top-right); and after irradiation up to $1 \times 10^{16}\,n_{eq}\,cm^{-2}$ for $50 \times 50\,\mu m^2$ (bottom-left) and $25 \times 100\,\mu m^2$ (bottom-right). Sensors produced by FBK.

operational range of the sensor, defined with an overall efficiency larger than 97%. Consumption has been evaluated operating the sensors at around $-25\,°C$, and for both geometries $50 \times 50\,\mu m^2$ and $25 \times 100\,\mu m^2$. Fig. 8 summarizes the results detailed in [20, 23].

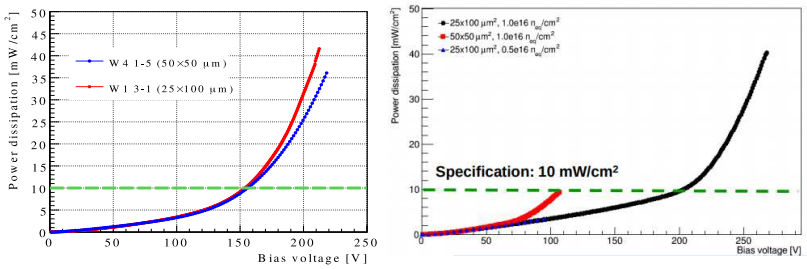


Fig. 8. Sensor power dissipation with respect to the operating bias voltage for 25x100 and 50x50 geometries, irradiated up to $1 \times 10^{16}\,n_{eq}\,cm^{-2}$ and operated with a temperature around $-25\,°C$. Figure on the left corresponds to SOI IMB-CNM of 150 µm thick sensors; on the right, FBK SiSi 150 µm thick using the Stepper lithography mask.

3. Conclusions

Small-pitch 3D pixel sensors bump-bonded to the pre-production ROC RD53A have proven to have an excellent radiation tolerance up to $1 \times 10^{16}\,n_{eq}\,cm^{-2}$, keeping hit efficiency larger than 97% at particle normal incidence with operational bias voltages below 200 V. This allows to fulfill the power dissipation specifications required by the ATLAS and CMS detectors.

Both geometries being considered, $25 \times 100\,\mu m^2$ and $50 \times 50\,\mu m^2$, show similar performance, in particular the $25 \times 100\,\mu m^2$ with 1 electrode is able to deal with the radiation tolerance demanding conditions, therefore there is no need for the 2 electrodes design. Their performance meets the baseline requirements to be qualified for the HL-LHC inner tracker upgrades of ATLAS and CMS.

A new set of test beam measurements is being planned for samples already irradiated to $2 \times 10^{16}\,\mathrm{n_{eq}\,cm^{-2}}$, while further irradiation are planned to reach the expected fluences for the LS5, i.e. $2.6 \times 10^{16}\,\mathrm{n_{eq}\,cm^{-2}}$, when is planned the replacement of the modules of the innermost layers of CMS. New productions of sensors bump-bonded to the experiment-dedicated ROCs, the ItkPixV1 (ATLAS) and the CROC (CMS) have already started.

References

[1] G. Apollinari et al., *High-Luminosity Large Hadron Collider (HL-LHC): Preliminary Design Report*, CERN Yellow Reports: Monographs, doi:10.23731/CYRM-2017-004 (2017).

[2] The CMS Collaboration, *The Phase-2 Upgrade of the CMS Tracker - Technical Design Report*, CERN-LHCC-2017-009, CMS-TDR-014 (2017).

[3] The ATLAS Collaboration, *Technical Design Report for the ATLAS Inner Tracker Pixel Detector*, CERN-LHCC-2017-021, ATLAS-TDR-030 (2017).

[4] S. J. Parker et al., *3D- A proposed new architecture for solid-state radiation detectors*, Nucl. Instrum. Meth. A **395** 328 (1997).

[5] G. Pellegrini et al., *3D double sided detector fabrication at IMB-CNM*, Nucl. Instrum. Meth. A **699** (2013) 27.

[6] G. Pellegrini et al., *3D-Si single sided sensors for the innermost layer of the ATLAS pixel upgrade*, Nucl. Instrum. Meth. A **924** (2019) 69-72.

[7] ATLAS IBL Collaboration, *Prototype ATLAS IBL Modules using the FE-I4A Front-End Readout Chip*, JINST **7** (2012) P11010.

[8] ATLAS Collaboration, *Technical Design Report for the ATLAS Forward Proton Detector*, CERN-LHCC-2015-009, ATLAS-TDR-024, (2015).

[9] CMS and TOTEM Collaborations, *CMS-TOTEM Precision Proton Spectrometer*, CERN-LHCC-2014-021, TOTEM-TDR-003, CMS-TDR-13 (2014).

[10] M. Garcia-Sciveres, *The RD53A Integrated Circuit*, CERN-RD53-PUB-17-001 (2017).

[11] M. Moll, *RD50 Status Report*, 139th LHCC Meeting, http://cern.ch/go/SQl7, Accessed: 2020-11-16.

[12] G. Casse and M. Moll, *RD50 Prolongation Request 2018*, CERN-LHCC-2018-017. LHCC-SR-007 (2018).

[13] M. Manna et al., *First characterisation of 3D pixel detectors irradiated at extreme fluences*, Nucl. Instrum. Meth. A **979** (2020) 164458.

[14] A. Garcia Alonso et al., *Test beam characterization of irradiated 3D pixel sensors*, Contribution to 21st iWoRiD https://indico.cern.ch/event/774201/contributions/3429263/ (2019).

[15] J. Duarte-Campderros, *Study of 3D pixel sensors after non-uniform proton irradiation*, Contribution to TREDI2020 https://indico.cern.ch/event/813597/contributions/3727824/ (2020).

[16] I. Vila Alvarez et al., *Update on CSIC activities on LGAD & 3D sensors*, Contribution to 4th AIDA-2020 Anual Meeting http://cern.ch/go/7RGX (2019).

[17] *AD, PS and SPS Users Schedules*, Web page https://ps-sps-coordination.web.cern.ch/ps-sps-coordination/pindex.html Accessed 2020-11-18.

[18] R. Diener et al., *The DESY II test beam facility*, Nucl. Instrum. Meth. A **922** (2019) 265-288.

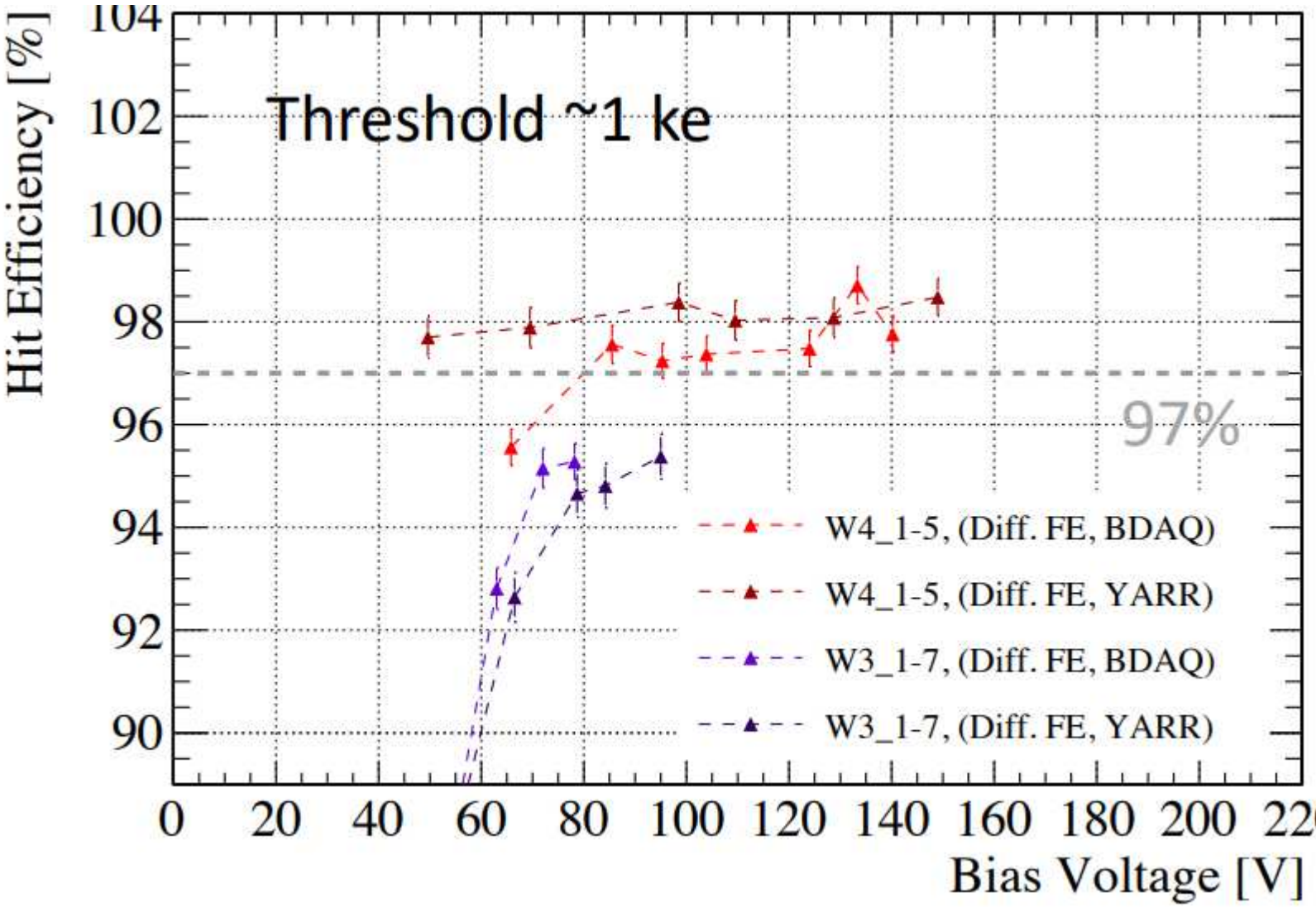
[19] I. Rubinskiy, on behalf of EUDET, AID Aconsortia, *An EUDET/AIDA Pixel Beam Telescope for Detector Development*, Phys. Procedia **37** (2012) 923-931.

[20] S. Terzo et al., *A new generation of radiation hard 3D pixel sensors for the ATLAS upgrade*, Nucl. Instrum. Meth. A **982** (2020) 164587.

[21] J. Duarte-Campderros et al., *Results on proton-irradiated 3D pixel sensors interconnected to RD53A readout ASIC*, Nucl. Instrum. Meth. A **944** (2019) 162625.

[22] M. Meschini et al., *Radiation resistant innovative 3D pixel sensors for the CMS upgrade at the High Luminosity LHC*, Nucl. Instrum. Meth. A **978** (2020) 164429.

[23] A. A. Samy et al., *Characterization of FBK 3D Pixel Sensor Modules Based on RD53A Readout Chip for the ATLAS ITk*, Contribution to TREDI2020, https://indico.cern.ch/event/813597/contributions/3727841 (2020).


Threshold ~1 ke
Hit Efficiency [%]
Bias Voltage [V]
97%
W4_1-5, (Diff. FE, BDAQ)
W4_1-5, (Diff. FE, YARR)
W3_1-7, (Diff. FE, BDAQ)
W3_1-7, (Diff. FE, YARR)
104
102
100
98
96
94
92
90
0
20
40
60
80
100
120
140
160
180
200
220